

INELASTIC PION-NUCLEON SCATTERING FROM 720 to 1180 MeV/c*

by

A. D. Brody, A. Kernan, ** D. W. G. S. Leith,
B. S. Levi, A. Minten, *** and B. C. Shen

Stanford Linear Accelerator Center
Stanford University, Stanford, California

and

P. Berge, / D. Herndon, R. Longacre, L. Price,
A. H. Rosenfeld and P. Soding

Lawrence Radiation Laboratory
University of California, Berkeley, California

I. Introduction

The extensive phase shift analyses of πp elastic scattering carried out over the last few years have suggested very complex behaviour of many of the partial wave amplitudes.¹ In addition, most of these amplitudes appear to be rather inelastic. The motivation for the experiment, therefore, is to carry out an extensive systematic study of πp inelastic scattering in order to determine the branching ratios of the various nucleon isobars into inelastic channels and to provide a more complete understanding of the πp interaction.

* Work performed under the auspices of the U. S. Atomic Energy Commission.

** Present address Dept. of Physics, U.C. Riverside, Riverside, California

*** Present address T. C. Division, CERN, Geneva

/ Present address Nuclear Physics Laboratory, Oxford University
Oxford, England

(Presented at XIVth International Conference on High Energy Physics,
August 28 - September 5, 1968, Vienna, Austria)

The experiment will eventually cover the range from 450 to 2000 MeV/c, in approximately 40 MeV/c steps. The scope of the experiment is illustrated in Fig. 1. In this paper we wish to report a preliminary study of the data from 720 to 1180 MeV/c where we have analyzed approximately 100,000 2-prong events, representing about 50% of the existing measurements. A further 200,000 events are being measured in the higher momentum region.

In section II we discuss the procedures involved in the analysis of the data. In section III we discuss the data for the elastic and inelastic scattering reactions. Finally, in section IV, we present a preliminary discussion on interpretation of the data.

II. Data Processing

We have used exposures taken with the 72" Alvarez hydrogen bubble chamber and the 30" MURA hydrogen bubble chamber. The film was scanned twice and the 2-prong events were measured on the Berkeley Spiral Reader, after which they were processed through the POOH-TVGP-SQUAW-ARROW system of programs.

The measuring and filtering efficiency of the system was estimated from a sample of $\sim 17,000$ events which were measured twice. The success rate was found to be 92% percent after one measurement and better than 99% after measurement of the failures. We conclude therefore that our total sample is unbiased since the failures appear to be random.

The reaction channels were first separated on the basis of the kinematical χ^2 for each hypothesis, always preferring the four-constraint

elastic scattering fit to the other one-constraint hypotheses. The remaining ambiguities among one-constraint fits amounted to 15% of the data and this was reduced to less than 1% by using the ionization χ^2 obtained by an analysis of the pulse height measurements by the Spiral Reader. The selection criteria applied are as follows:

a. 4C elastic fits:

accepted if χ^2 (kinematic) ≤ 14 ,

b. 1C $n\pi^+\pi^- / p\pi^-\pi^0$ unique fits:

accepted if χ^2 (kinematic) ≤ 7 ,

c. 1C $n\pi^+\pi^- / p\pi^-\pi^0$ ambiguous fits:

(1) accepted if $[\chi^2$ (bubble) of $n\pi^+\pi^- / p\pi^-\pi^0] \leq [\chi^2$ (bubble) of $p\pi^-\pi^0 / n\pi^+\pi^- - 3]$,

(2) accepted if difference between χ^2 (bubble) for these two channels is less than 3 but $[\chi^2$ (kinematic) of $n\pi^+\pi^- / p\pi^-\pi^0] \leq [\chi^2$ (kinematic) of $p\pi^-\pi^0 / n\pi^+\pi^- - 1.5]$,

(3) accepted if above tests fail to distinguish between ambiguities but $[\chi^2$ (bubble) of $n\pi^+\pi^- / p\pi^-\pi^0] \leq [\chi^2$ (bubble) of $p\pi^-\pi^0 / n\pi^+\pi^-]$.

Applying the above procedures we obtain the following samples:

$\pi^- p \rightarrow \pi^- p$	41,264 events
$\pi^- p \rightarrow \pi^+\pi^- n$	21,563 events
$\pi^- p \rightarrow p\pi^-\pi^0$	14,247 events

The χ^2 distribution biases, topological measurement biases, and scanning biases for each channel are treated as described below.

III. Data Analysis

a. Elastic Scattering:

The 41,264 elastic scattering events obtained as described above were corrected for the loss of short protons due to the azimuthal scanning bias and also for the χ^2 cutoff used in their selection. These corrections were applied at each momentum and at each production angle separately. We show in Fig. 2 the elastic scattering differential cross sections for 12 energies between 1500 and 1770. The curves through the data points are the best fits using a Legendre polynomial expansion where the fits were performed up to the 6th order. The expansion coefficients agree very well with those obtained by Duke *et al.*³ throughout this same energy region. The absolute normalization for these plots together with the total elastic cross section is obtained by normalizing our data to the central region of the elastic scattering data as measured by the counter experiments.³ That is, we compare the fit to our angular distributions in their region of production angle from $-.8$ in $\cos \theta$ through to $+.7$ and normalize our relative angular distribution with respect to the absolute counter data points in the same angular region. The total elastic scattering cross section was then obtained by fitting to all of our angular distribution data and normalizing the relative yield by the above number. This is shown in Fig. 3 as a function of energy and is plotted together with the data of other counter experiments. As can be seen readily, the agreement is rather good. It is noteworthy that the cross section of this central region used for our normalization varies very slowly with energy throughout this region, and that the rapid variation in the total elastic

cross section seen in Fig. 3 is almost entirely due to the forward and backward scattering peaks not used in our normalization. It is also interesting to note that the normalization region represents 20-30% of the total data in the angular distribution. Therefore the agreement between our data and the counter data is a measure of how well we measure the elastic scattering distribution. We show in Fig. 4 the forward elastic scattering differential cross section obtained by extrapolating our best Legendre polynomial fit to the forward direction. Again our points compare very well with those points obtained by using the dispersion relation calculations⁴ which are also shown in Fig. 4.

We have used the elastic scattering measurements so far only in the cross section normalization and have not yet used this data in our preliminary phase shift analysis, nevertheless we plan to incorporate elastic scattering data together with inelastic scattering data in our complete fits shortly.

b. Inelastic Reactions:

As described above, we have identified 21,563 events of the type $\pi^- p \rightarrow n\pi^+\pi^-$ and 14,247 events of the type $\pi^-\pi^0 p$. This data has also been corrected for scanning biases and the χ^2 cutoff, which amounted to about 5%, and are constant with respect to the production angle.

The reaction cross sections are shown in Figs. 5 and 6 for $\pi^-\pi^+n$ and $\pi^-\pi^0 p$ reactions, respectively. Here again the same normalization

procedure as described earlier has been used in obtaining the cross sections. Also shown in these figures for comparison are the existing measurements of other experiments.⁵ Figs. 7 and 8 show our data separately. Due to the better statistics and the most systematic coverage of this energy region, our measurements reveal more concretely the detailed structure in the cross sections. The discrepancies between the measurements in the 72" LRL chamber and the 30" MURA chamber is possibly due to the preliminary nature of the data analysis of the MURA chamber film at present. We hope to complete our analysis of 30" MURA HBC film and also to include measurements near 1600 MeV and 1720 MeV regions in the near future.

The reaction $\pi^- \pi^+ n$ is dominated by strong $\Delta^-(1236)$ production as illustrated by a typical Dalitz plot at the energy 1685 MeV in Fig. 9. The contributions of the quasi two-body processes

$$\begin{aligned}\pi^- p &\rightarrow \pi^+ \Delta^- \\ &\rightarrow \pi^- \Delta^+ \\ &\rightarrow \rho^0 n\end{aligned}$$

have been evaluated using a maximum likelihood program MURTEBERT,⁶ assuming the reaction $\pi^- \pi^+ n$ is an incoherent superposition of these resonant channels together with phase space. We show in Fig. 10 (a)-(c) a typical set of spectra for the square of the effective mass of $n\pi^-$, $n\pi^+$, and $\pi^+ \pi^-$ respectively, at the energy of 1685 MeV. The curves represent the best fits to the data with contributions of 57.6 percent $\pi^+ \Delta^-$, 7.2 percent $\pi^- \Delta^+$, 0.3 percent $\rho^0 n$, and the rest being 3-body phase space. The masses and the widths of the resonances are fixed in this

fit to be $M(\Delta) = 1236$ MeV, $\Gamma(\Delta) = 130$ MeV.

$$M(\rho) = 765 \text{ MeV}, \quad \Gamma(\rho) = 130 \text{ MeV}.$$

In Fig. 11 we show the cross sections for the channel $\pi^+ \Delta^-$ over our energy region, where we have used the above fractions obtained from the likelihood fit to determine that portion of the Δ^- present. It is clear that this reaction shows an enhancement in the region of 1680 MeV, and this may be associated with the decay of one or both of the D_{15} , F_{15} resonances into the $\Delta\pi$ channel.

The overall center of mass production angular distributions for the outgoing π^+ with respect to the incident π^- have been examined in terms of Legendre polynomial expansions with the resulting coefficients shown in Fig. 12. All existing data from all other experiments are also shown in Fig. 12 for comparison.⁷ It is evident that our points match very well with other experiments. We further investigate the production angular distributions of the quasi two-body $\pi^+ \Delta^-$ channel by selecting events with $1140 \text{ MeV} \leq M(n\pi^-) \leq 1320 \text{ MeV}$. In Fig. 13 we show these production angular distributions which demonstrate noticeable changes in the energy regions 1500 to 1650 MeV and 1690 to 1770 MeV. We show in Fig. 14 the corresponding Legendre polynomial expansion coefficients of these distributions. It is interesting to note that there is very little structure in the angular distribution coefficients throughout that region where the elastic and the inelastic cross sections show a rather large peak. There is, however, clear evidence of activity around the 1520 MeV region in $\Delta\pi$ angular distribution, despite the fact that the cross section shows no strong structure.

The flatness of the Legendre coefficients throughout the 1600-1700 MeV region implies that whatever amplitudes dominate this bump region must have roughly constant phase differences in this region (since activity in these coefficients are directly proportional to the rate of change of the phase angle between any two interfering amplitudes).

The alignment of the Δ^- is studied by examining the Adair angular distribution for the decay of the Δ . These are shown in Fig. 15 where the data is averaged over all production angles of the Δ .

Since we have established above that the rate of change of the phase angle between the various amplitudes contributing in this region must be small, and since the cross section does not show two separate bumps in this region, we do not expect a large polarization term in the interference of the amplitudes, and therefore do not suspect strong alignment of the Δ . To investigate more fully we show the same Adair angular distributions for Δ decay for those events produced at small angles. These data are shown in Fig. 16, where some evidence of structure may be seen in the regions around 1660 MeV, and around 1700 MeV. These are not yet completely understood.

IV. Interpretation of Data

Starting from the well established resonances we may deduce a qualitative picture of the πp interaction in the region by inspecting the Legendre coefficients displayed in Fig. 14.

The region from 1500-1600 MeV will be dominated by the D_{13} (1520); from 1600-1700 the D_{15} (1680) and F_{15} (1690) will take over and finally above 1700 we expect some effect due to the low energy tail of the

$F_{37}(1920)$. If we assume that we have a genuine quasi-two body final state it is possible to relate the contributions from the interferences of the partial wave amplitudes to the Legendre coefficients. The contributions from the dominant waves are shown in Table I. The table assumes that $|SS^*| = 1$.

Between 1500 and 1600 we expect the interference of the $D_{13}(1520)$ with the two spin 5/2 resonances to contribute positively to A_1 and A_2 . In fact we find strong negative contributions decreasing as the energy increases. This would imply that the D_{13} couples with a negative relative sign to the F_{15} and D_{15} .

The behavior of the coefficients between 1600 and 1700 MeV is consistent with the presence of the two spin 5/2 resonances. The absence of any dramatic variation of A_3 and A_1 suggests that the phase difference between these two amplitudes changes very slowly, confirming the results of the elastic scattering data. Above 1700 MeV we do not have sufficient information except to say that the upward trend of A_1 together with the negative A_6 could be at least partially due to the tail of the $F_{37}(1920)$ which is only one full width away.

With this input information we have attempted to make a partial wave fit using the three resonances $D_{13}(1520)$, $D_{15}(1680)$, and $F_{15}(1690)$ with masses and widths as quoted in the "Rosenfeld" Tables by Barash-Schmidt et al.⁸ In addition, we added s, p, d, and f wave backgrounds. The resonances are parameterized by Breit-Wigner forms while the backgrounds used are of the type $a + b(p_{c.m.})$ where a and b are complex numbers. All parameters, including resonant masses and widths, are allowed to vary.

The results, which gave a χ^2 of 286 for 252 data points and 23 parameters, are shown in Table II. Using the elasticities quoted by Lovelace for the three resonances, we obtain the following branching fractions:

$$\frac{D_{13}(1520) \rightarrow \Delta\pi}{\text{ALL}} = .12$$

$$\frac{D_{15}(1680) \rightarrow \Delta\pi}{\text{ALL}} = .15$$

$$\frac{F_{15}(1690) \rightarrow \Delta\pi}{\text{ALL}} = .19$$

We have also succeeded in fitting the same data by just using the resonances suggested by Lovelace between 1500 and 1750 MeV (except for the $S_{11}(1535)$ and $S_{11}(1710)$). The χ^2 for this fit is 330 for 252 data points and 24 parameters. The results are shown in Table III.

We must emphasize again that these two fits are not to be considered final in any sense, but serve only to illustrate our quasi two body approach to the understanding of the πp interaction. Currently we are exploring the approach further with various different parameterizations and systematic searches. We shall shortly extend our program to use more sophisticated models analysing the entire Dalitz plot and to undertake some multi-channel analyses.

References

1. For a review on this subject see C. Lovelace, Nucleon Resonances and Low Energy Scattering, Rapporteur's talk at the 1967 Heidelberg Conference, CERN Report No. TH-837, October 1967; and C. Johnson and H. Steiner, Pion-Proton Elastic Scattering: Low Energy Experiments and Phase Shift Analyses, Invited paper presented by H. Steiner at the Conference on πN Scattering held at the University of California, Irvine, December 1-2, 1967, UCRL-18001.
2. P. J. Duke, D. P. Jones, M. A. R. Kemp, P. G. Murphy, J. D. Prentice, J. J. Thresher, Phys. Rev. 142, 1077 (1966).
3. J. A. Helland, C. D. Wood, T. J. Devlin, D. E. Hagge, M. J. Longo, B. J. Moyer, V. Perez-Mendez, Phys. Rev. 134, B 1079 (1964); and P. J. Duke et al., of ref. 2.
4. We have used the forward differential cross sections obtained by using dispersion relation calculations as quoted by Duke et al., and Helland et al. of refs. 2 and 3.
5. L. Bertanza, A. Bigi, R. Carrara and R. Casali, Nuovo Cimento 44, 712 (1966).
R. A. Burnstein, G. R. Charlton, T. B. Day, G. Quarenii, A. Quarenii-Vignudelli, G. B. Yodh and I. Nadelhaft, Phys. Rev. 137, B 1044 (1964).
N. M. Cason, I. Derado, J. W. Lansa, V. P. Kenney, J. A. Poirier, W. D. Shephard, C. N. Vittitoe and J. L. Stautberg, Phys. Rev. 150, 1134, (1966).
R. R. Crittenden, H. J. Martin and B. Musgrave, Sienna International Conference on Elementary Particles, 1963, Vol. 1, p. 116.
S. Femino, S. Jannelli and F. Mezzanares, Nuovo Cimento 52, 892, (1967).
C. Gensollen, P. Granet, R. Barloutaud, A. Leveque, and J. Meyer, Sienna International Conference on Elementary Particles 1963, Vol. 1, p. 84.
J. Kirz, J. Schwartz and R. D. Tripp, Phys. Rev. 130, 2481, (1963).
J. D. Oliver, I. Nadelhaft and G. B. Yodh, Phys. Rev. 147, 932, (1966).
E. Pickup, D. K. Robinson, E. O. Salant, F. Ayer and B. A. Munir, Phys. Rev. 132, 1819, (1963).
C. N. Poirier, C. A. Tilger, E. D. Alyea, Jr., H. J. Martin, Jr., J. I. Rhodes, and J. H. Scandrett, Phys. Rev. 148, 1311, (1966).
C. N. Vittitoe, B. R. Riley, W. J. Fickinger, V. P. Kenney, J. G. Mowat, and W. D. Shephard, Phys. Rev. 135, B 232, (1964).
6. J. Friedman, MURTEBERT, A General Program for Fitting Data by the Method of Maximum Likelihood, Alvarez Programming Group Note No. P-156.

7. The Legendre coefficients are obtained by fitting the production angular distributions given in the papers of ref. 5.
8. N. Barash-Schmidt, A. Barbaro-Galtieri, L. R. Price, M. Ross, A. H. Rosenfeld, P. Soding, C. G. Wohl, Review of Particle Properties, UCRL 8030, July, 1968.

Figure Captions

1. The total and elastic $\pi^- p$ scattering cross sections as a function of laboratory incident momentum. Markers represent the momentum range covered by this experiment.
2. Elastic scattering differential cross sections at 12 energies. The curves correspond to the best fits to Legendre polynomial expansions.
3. Total elastic scattering cross section measured by this experiment and counter experiments of Duke *et al.*, and Helland *et al.*
4. Forward differential cross sections from this experiment and from calculations using dispersion relations.
5. Production cross section of $\pi^- p \rightarrow \pi^- \pi^+ n$ measured by this experiment and other experiments as listed in Ref. 5.
6. Production cross section of $\pi^- p \rightarrow \pi^- \pi^0 p$ measured by this experiment and other experiments as listed in Ref. 5.
7. Production cross section of $\pi^- p \rightarrow \pi^- \pi^+ n$ measured by this experiment.
8. Production cross section of $\pi^- p \rightarrow \pi^- \pi^0 p$ measured by this experiment.
9. A typical Dalitz plot for the reaction $\pi^- p \rightarrow \pi^- \pi^+ n$ at the c.m. energy of 1688 MeV.
10. Mass-squared distributions of $n\pi^-$, $n\pi^+$, and $\pi^+\pi^-$ for the reaction $\pi^- p \rightarrow \pi^- \pi^+ n$ at 1685 MeV. The curves correspond to the best fit in this reaction as described in the text.
11. Production cross section of the quasi-two body channel $\pi^- p \rightarrow \pi^- \Delta^- (1236)$.
12. Legendre polynomial expansion coefficients obtain in this experiment and other experiments as listed in Fig. 5 for the reaction $\pi^- p \rightarrow \pi^- \pi^+ n$.
13. Production angular distributions of the quasi-two body channel $\pi^- p \rightarrow \pi^- \Delta^-$ as selected with $1140 \text{ MeV} \leq M(n\pi^-) \leq 1320 \text{ MeV}$.
14. Legendre polynomial expansions to the distributions shown in Fig. 13.
15. The distributions of the Adair angle of the Δ^- over all production angles.
16. The distributions of the Adair angle of the Δ^- in the region of production angle $0.8 \leq \cos \Theta \leq 1.0$.

TABLE I

$\ell\ell'_{2J}$	$\lambda\lambda'_{2J}$	AA^X	A_0	A_1	A_2	A_3	A_4	A_5	A_6
DS3	DS3		2						
	DD5				3.2				
	FP5			6.5					
DD5	DD5		3		1.2		-2.9		
	DG5				-1.8		-4.5		
	FP5			1		4.2			
	FF5			1		3.2		-8.5	
FP5	FP5		3		2.4				
	FF5				-2.5		-6.3		
FF7	FF7		4		3.2		- .5		-4.4
	DD5			9.5		1.2		-7	
	FP5				2.1		5.4		

TABLE II

$$F_{15}: \quad \text{Mass} \quad = \quad 1690 \text{ MeV}$$

$$\text{Width} \quad = \quad 131 \text{ MeV}$$

$$\sqrt{X_e X_\Delta} (FP5) \quad = \quad 0.348$$

$$\sqrt{X_e X_\Delta} (FF5) \quad = \quad 0.025$$

$$D_{15}: \quad \text{Mass} \quad = \quad 1680 \text{ MeV}$$

$$\text{Width} \quad = \quad 170 \text{ MeV}$$

$$\sqrt{X_e X_\Delta} (DD5) \quad = \quad 0.245$$

$$\sqrt{X_e X_\Delta} (DG5) \quad = \quad 0.014$$

$$D_{13}: \quad \text{Mass} \quad = \quad 1520 \text{ MeV}$$

$$\text{Width} \quad = \quad 115 \text{ MeV}$$

$$\sqrt{X_e X_\Delta} (DS3) \quad = \quad - .264$$

Backgrounds

$$S \text{ wave} \quad = \quad (0.08 + .22 \times P_{cm}) + i (-.11 + .15 \times P_{cm})$$

$$P \text{ wave} \quad = \quad (-.09 - .03 \times P_{cm}) + i (.001 - .13 \times P_{cm})$$

$$D \text{ wave} \quad = \quad (.12 + .08 \times P_{cm}) + i (-.08 - .09 \times P_{cm})$$

$$F \text{ wave} \quad = \quad .013 - i \times .002$$

TABLE III

F_{15} : Mass = 1691 MeV

Width = 147 MeV

$\sqrt{X_e X_\Delta}$ (FP5) = 0.365

$\sqrt{X_e X_\Delta}$ (FF5) = 0.024

D_{15} : Mass = 1667 MeV

Width = 188 MeV

$\sqrt{X_e X_\Delta}$ (DD5) = .226

$\sqrt{X_e X_\Delta}$ (DG5) = .020

D_{13} : Mass = 1496 MeV

Width = 112 MeV

$\sqrt{X_e X_\Delta}$ (DS3) = - .386

P_{33} : Mass = 1730 MeV

Width = 273 MeV

$\sqrt{X_e X_\Delta}$ = - .15

S_{31} : Mass = 1634 MeV

Width = 179 MeV

$\sqrt{X_e X_\Delta}$ = - .09

D_{33} : Mass = 1679 MeV

Width = 269 MeV

$\sqrt{X_e X_\Delta}$ (DS3) = .165

$\sqrt{X_e X_\Delta}$ (DD3) = .053

P_{11} : Mass = 1752 MeV

Width = 329 MeV

$\sqrt{X_e X_\Delta}$ = .17

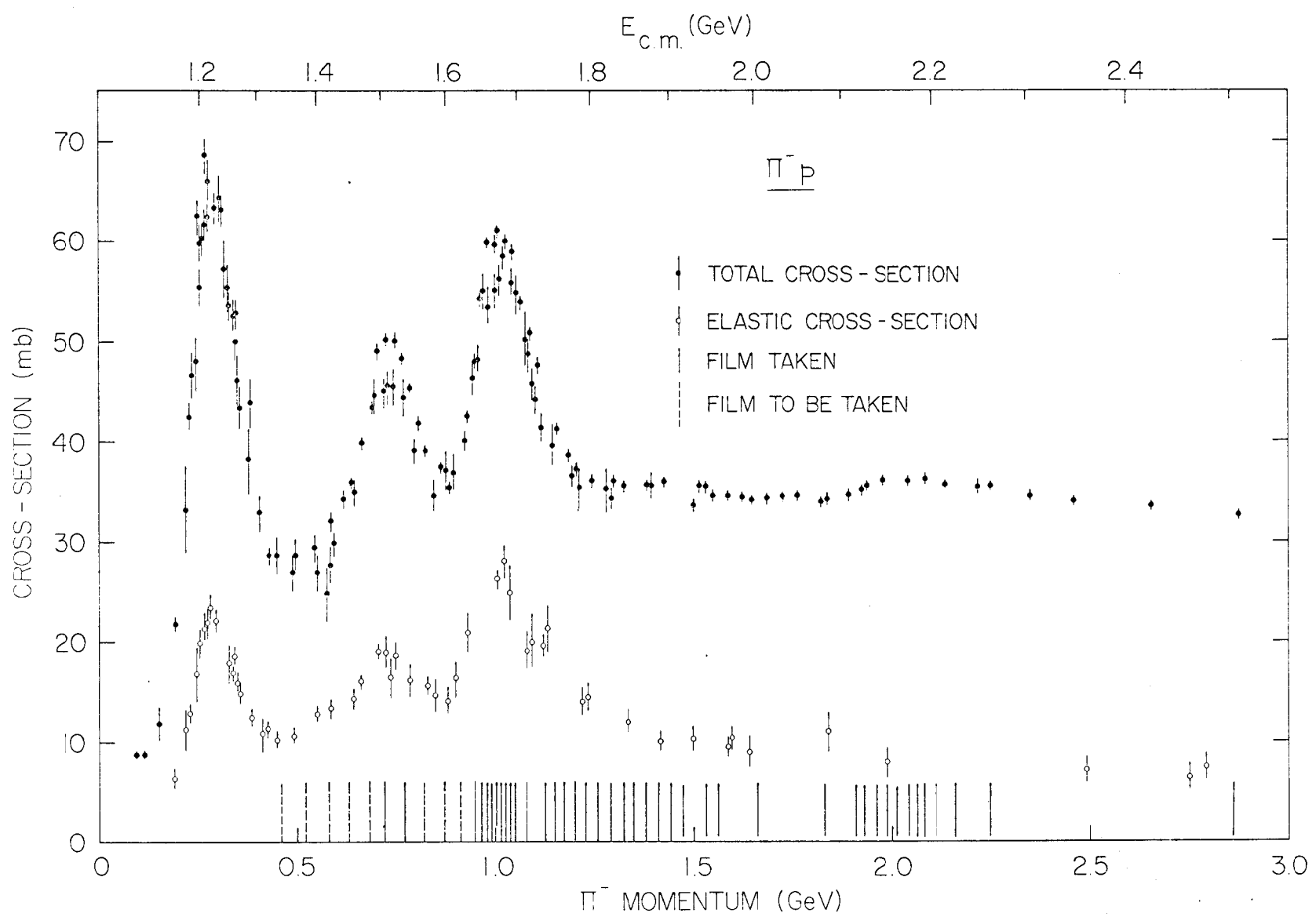


Fig. 1

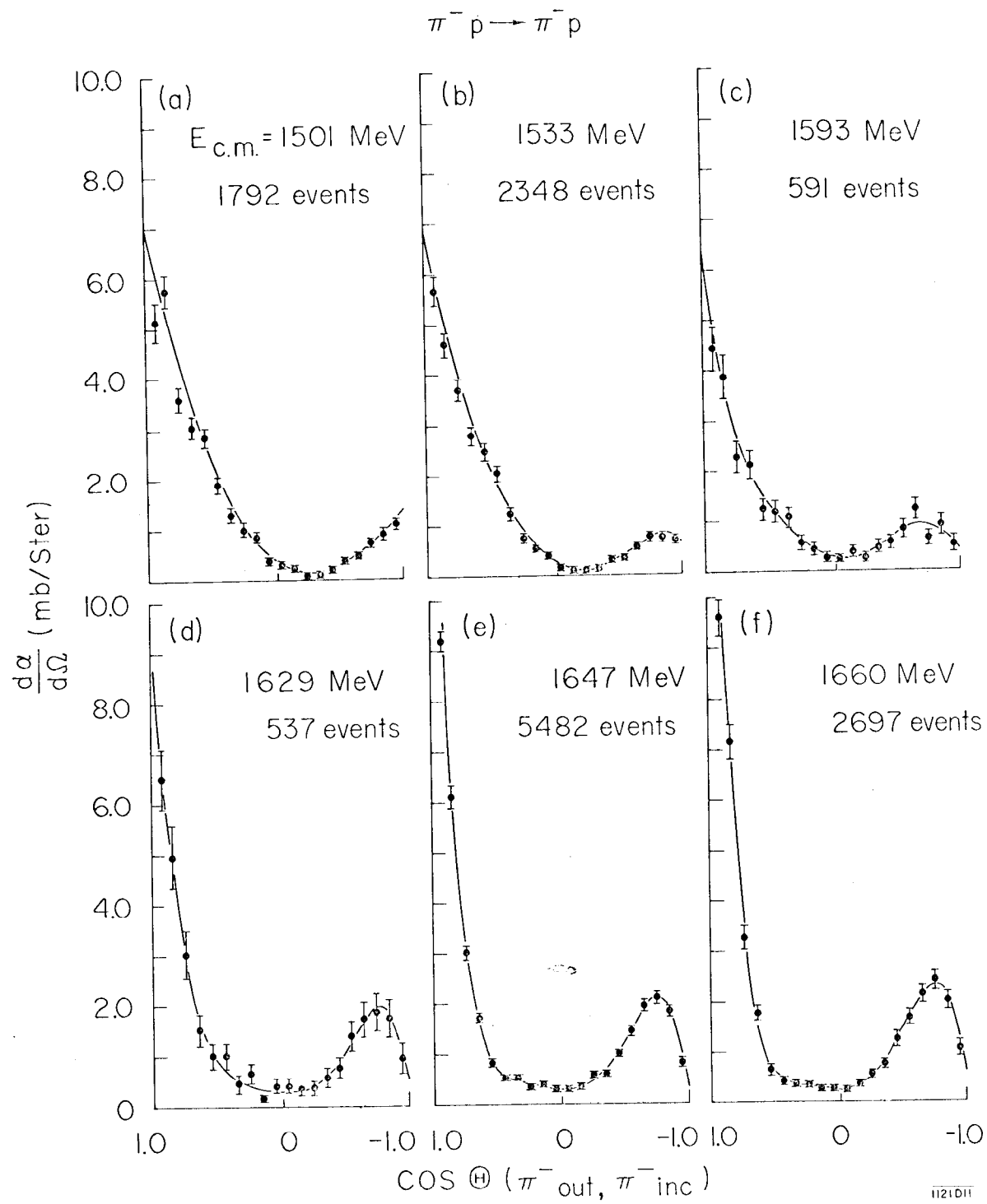


Fig. 2

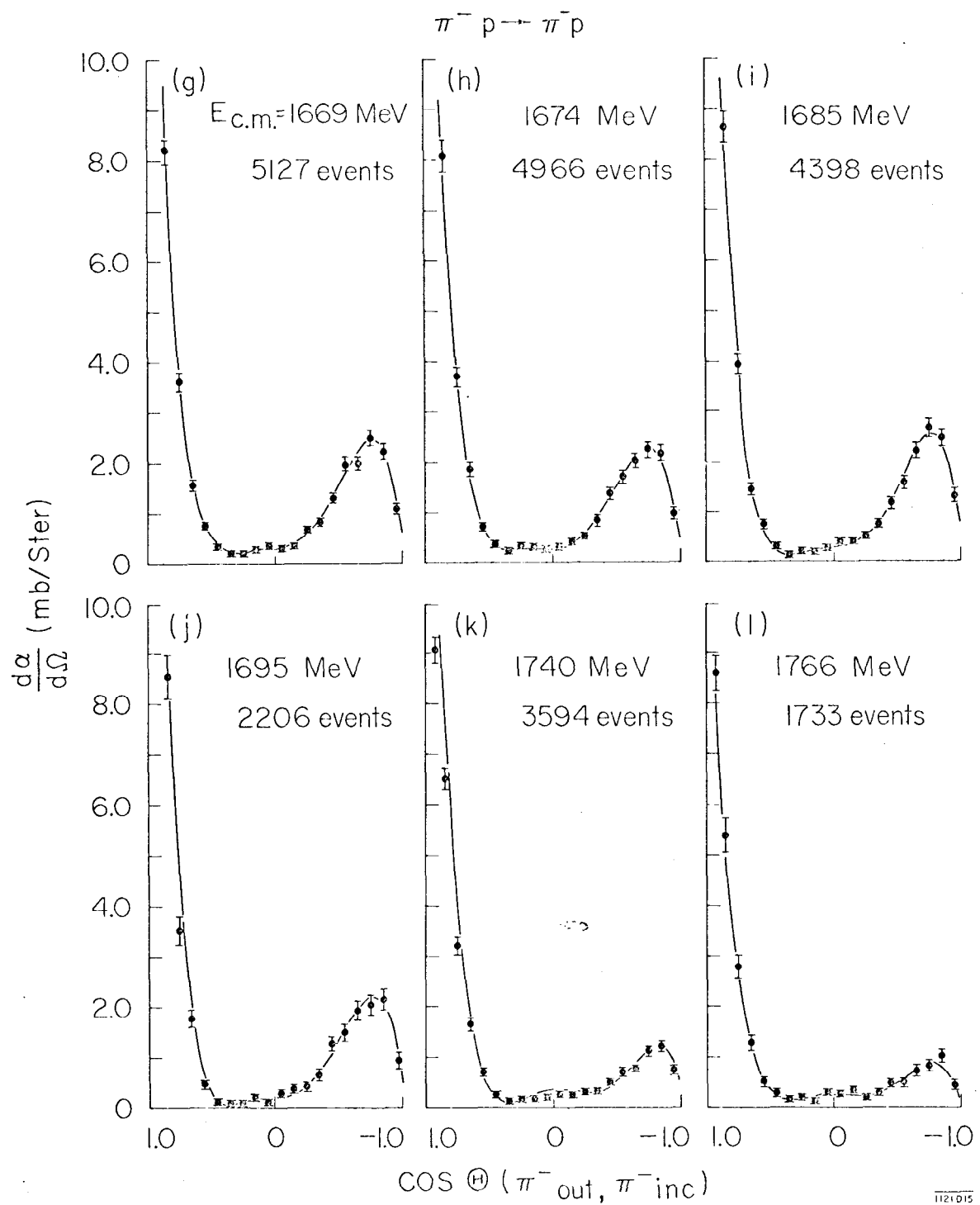


Fig. 2

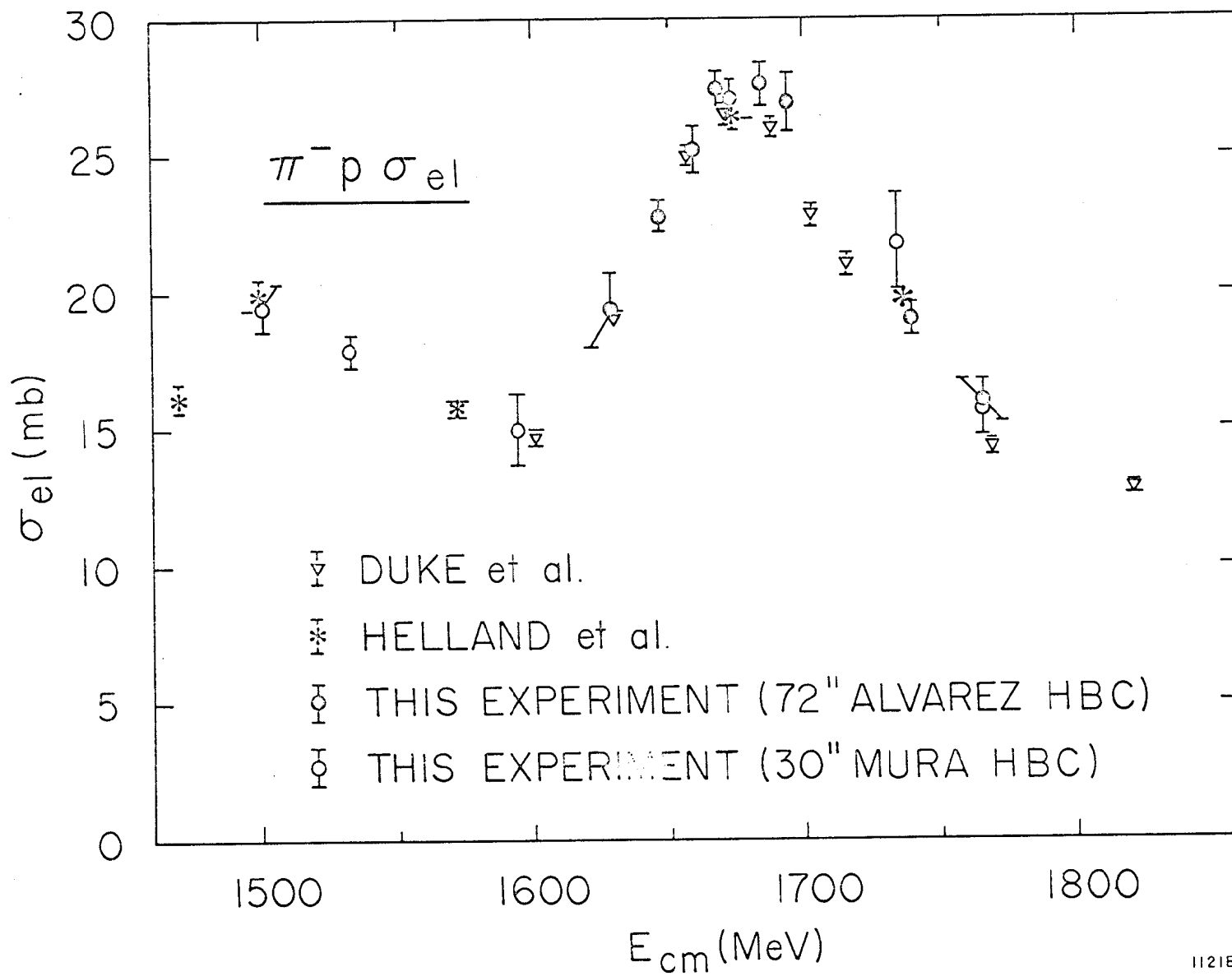
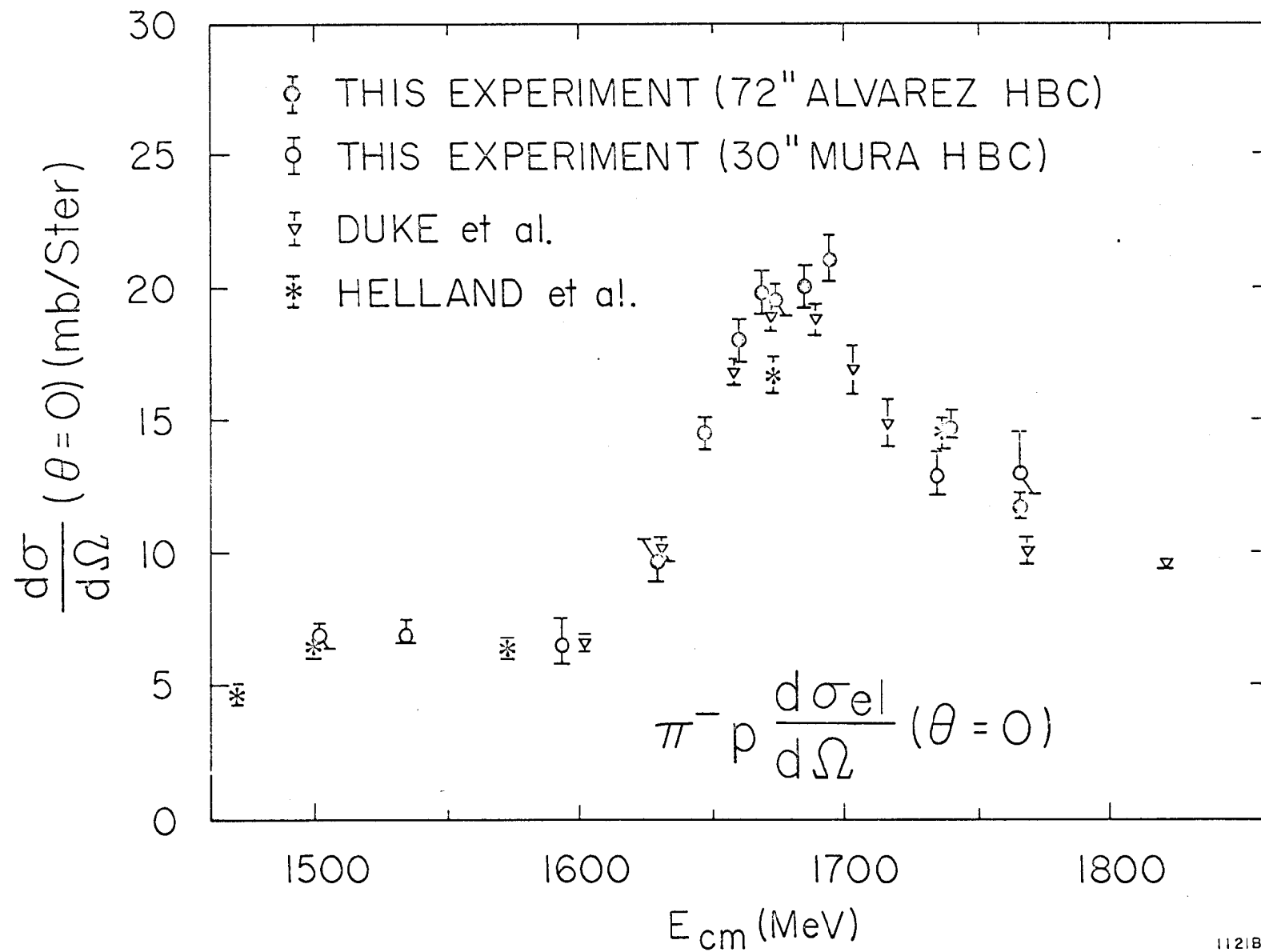


Fig. 3



112183

Fig. 4

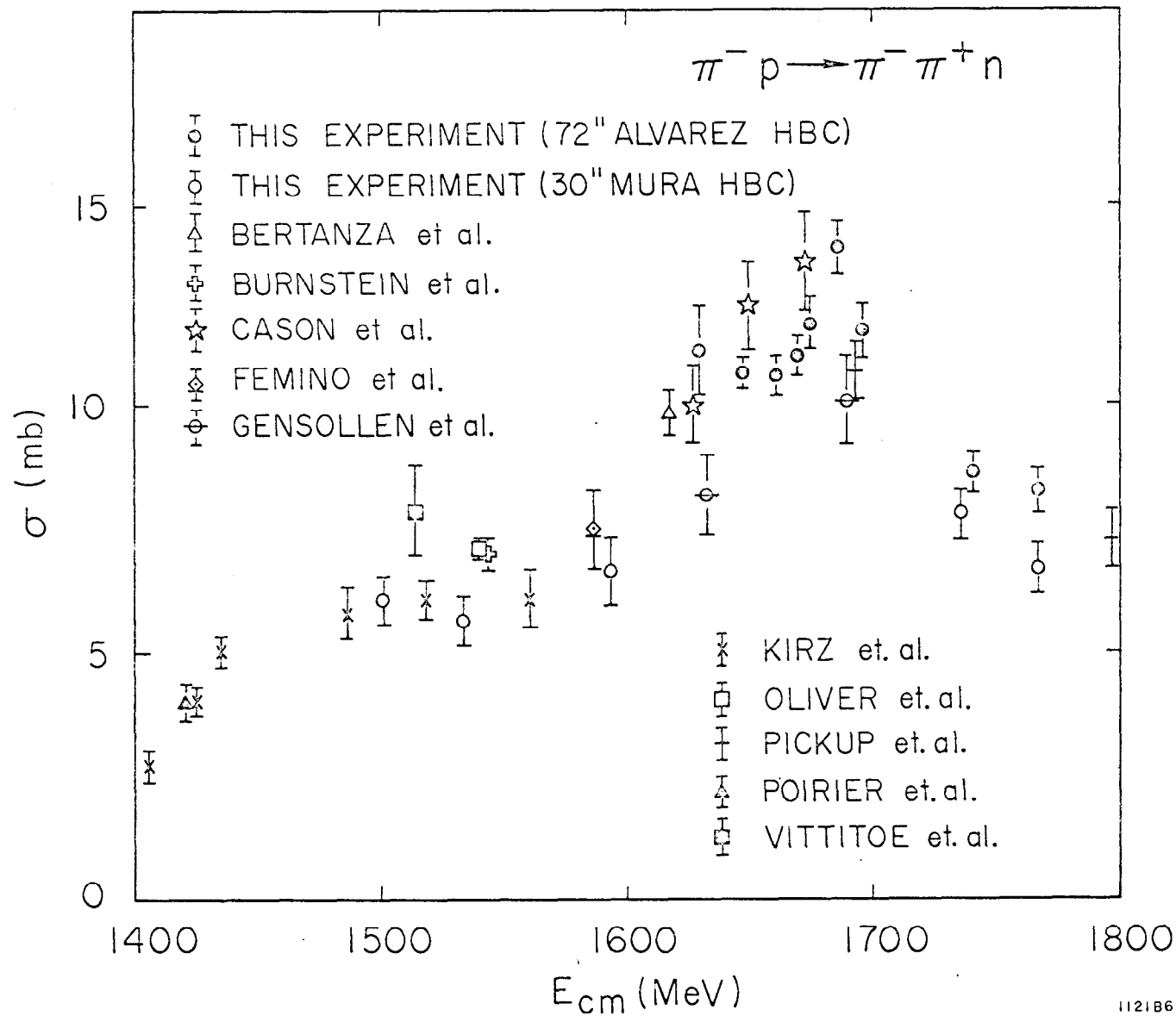


Fig. 5

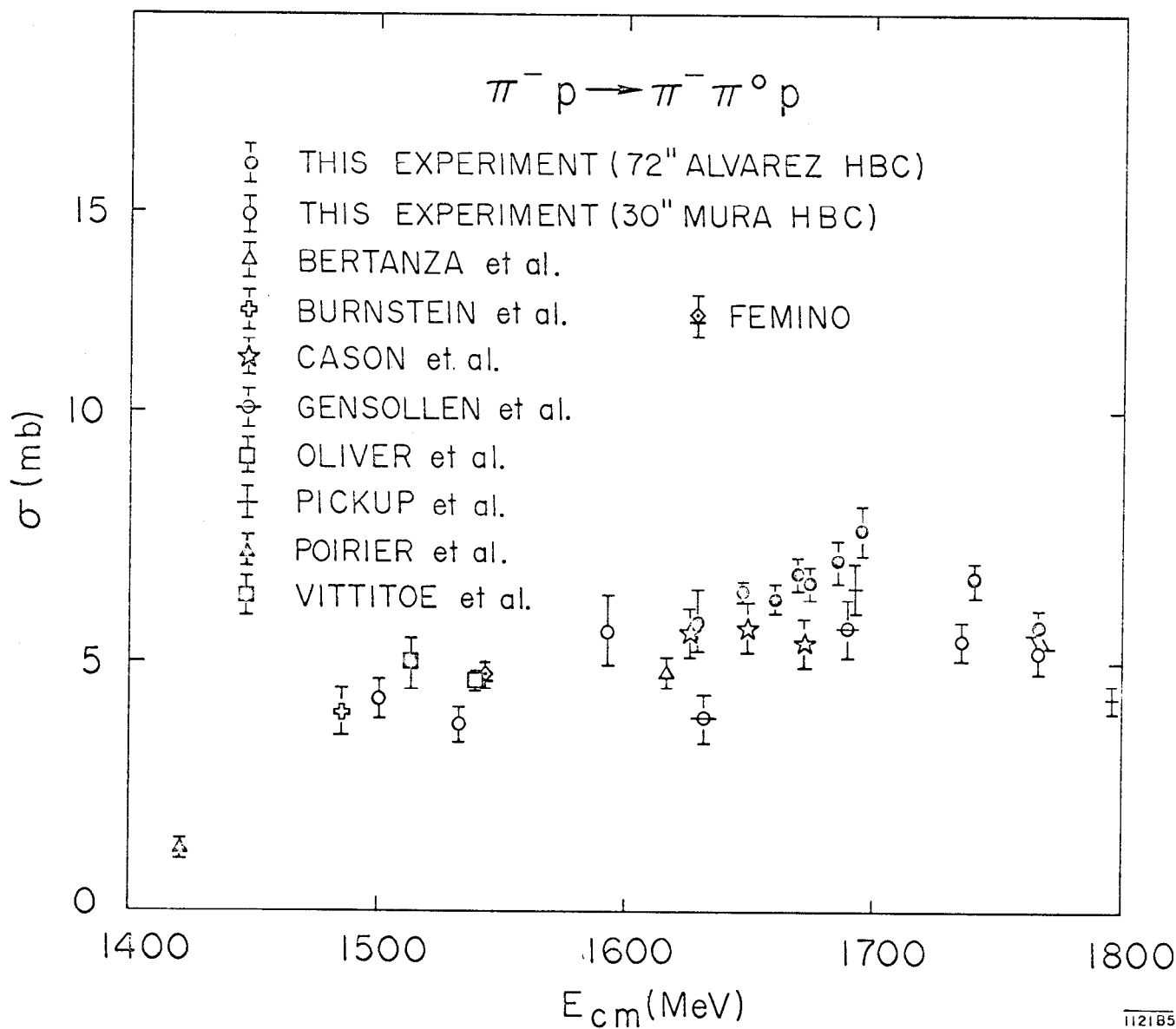
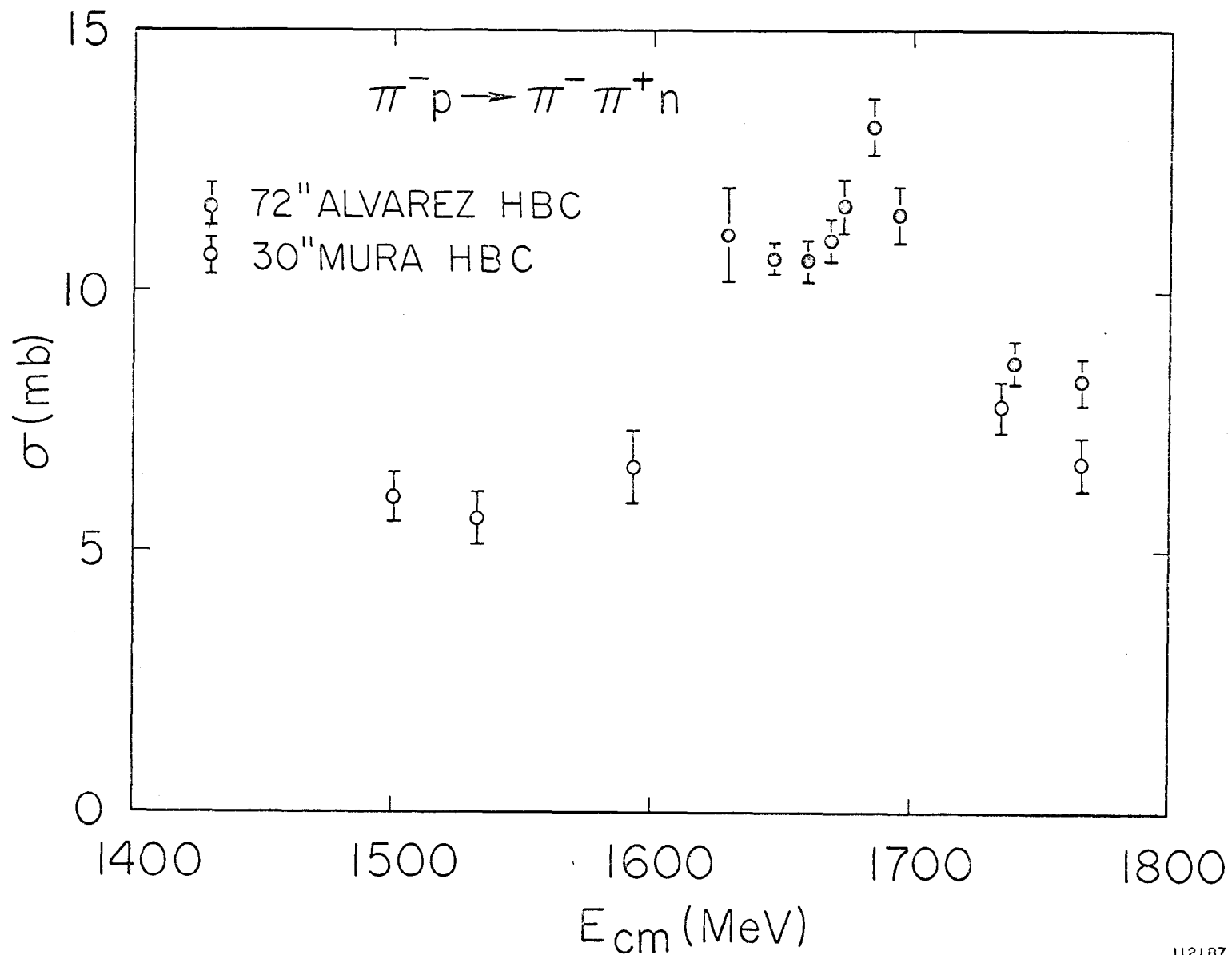


Fig. 6



112187

Fig. 7

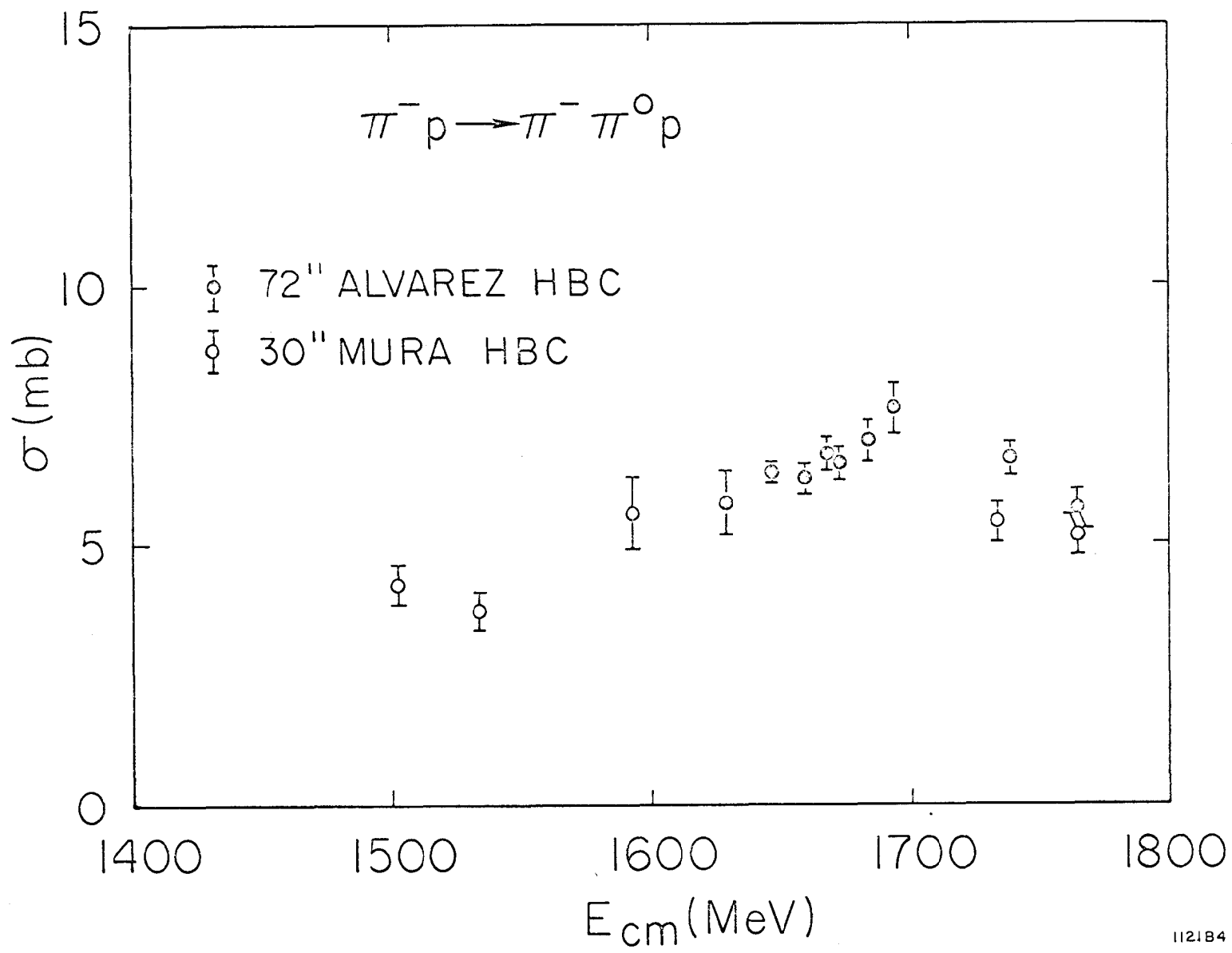


Fig. 8

112184

$$\pi^- p \rightarrow \pi^- \pi^+ n \quad 1688 \text{ MeV}$$

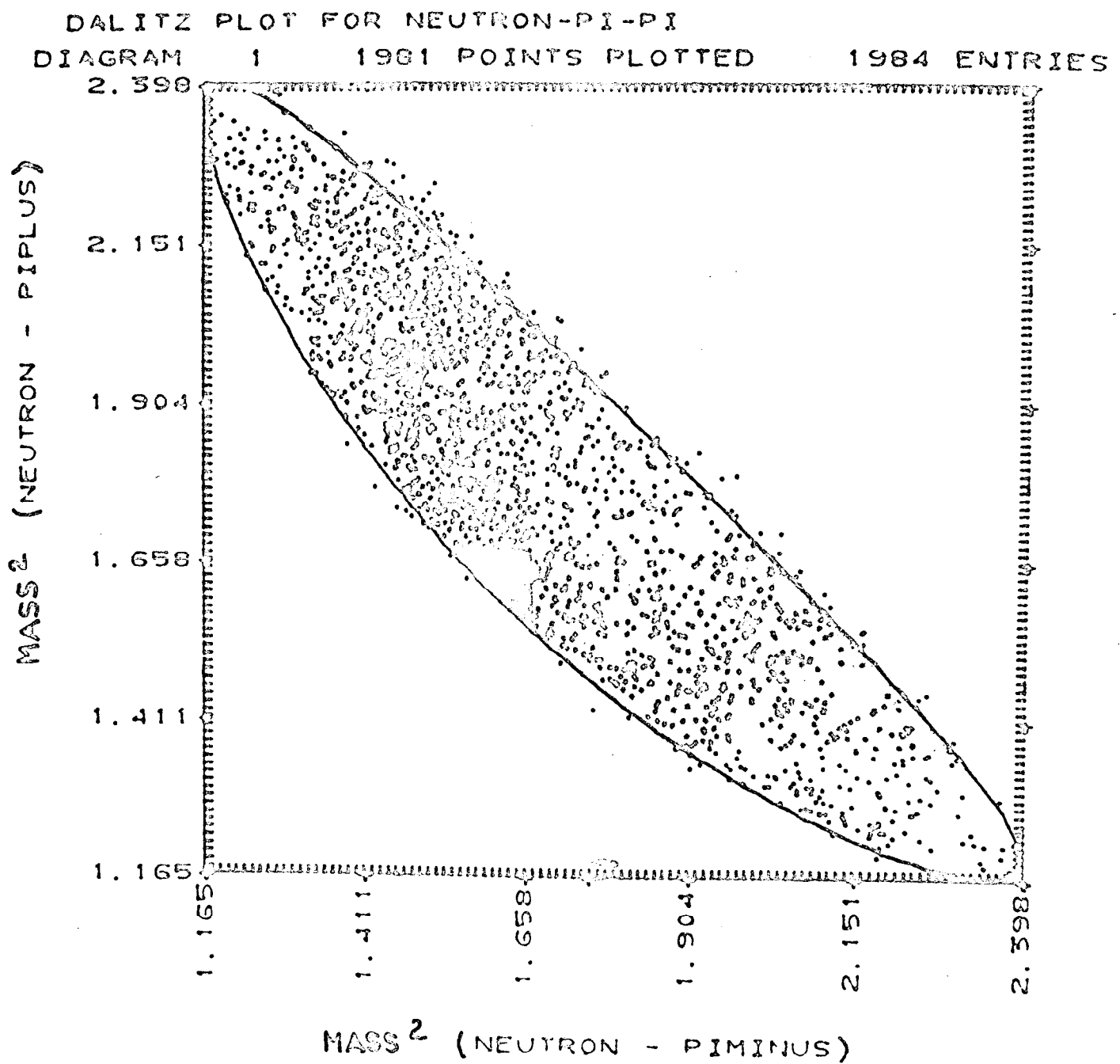


Fig. 9

$\pi^- p \rightarrow n \pi^+ \pi^-$
 $E_{c.m.} = 1685 \text{ MeV} \quad 2253 \text{ events}$

FIT:

$M(\Delta^-) = 1236 \text{ MeV} \quad 57.6 \%$

$M(\Delta^+) = 1236 \text{ MeV} \quad 72 \%$

$M(\rho^0) = 765 \text{ MeV} \quad 0.3 \%$

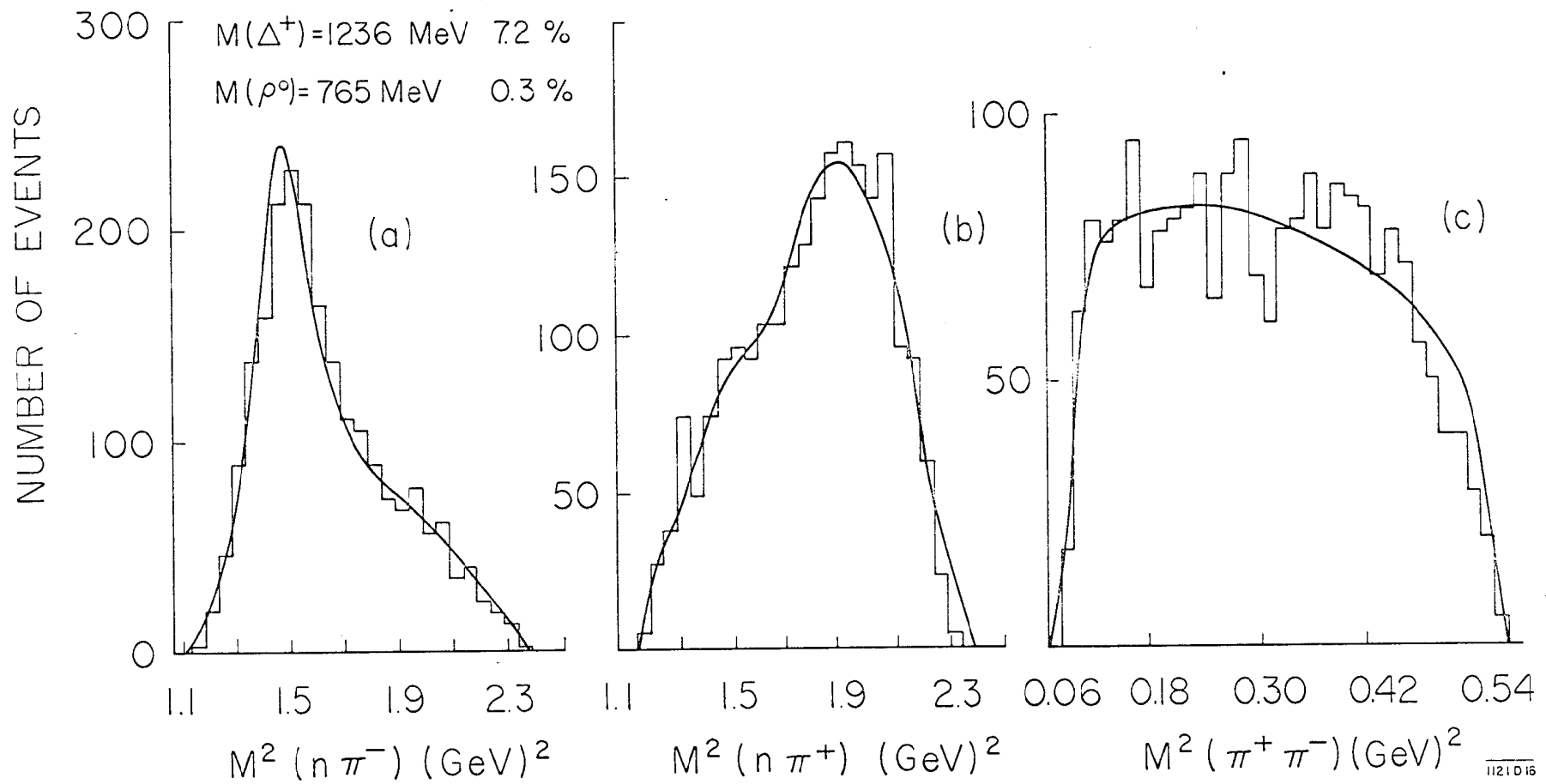


Fig. 10

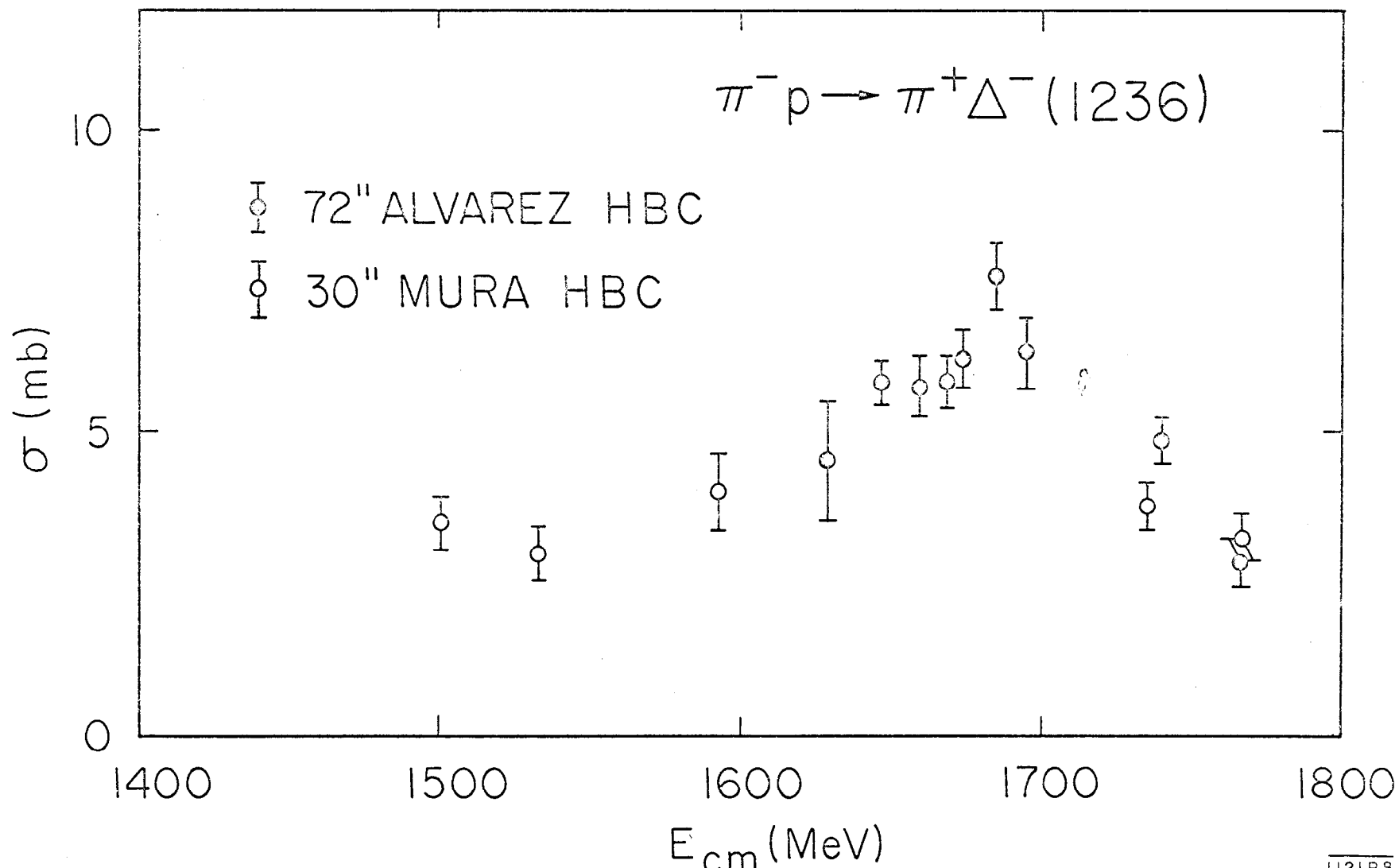


Fig. 11



$$\frac{d\sigma}{d\Omega} = \sum_{\ell} A_{\ell} P_{\ell}(\cos \Theta [\pi^+_{\text{out}}, \pi^-_{\text{inc}}])$$

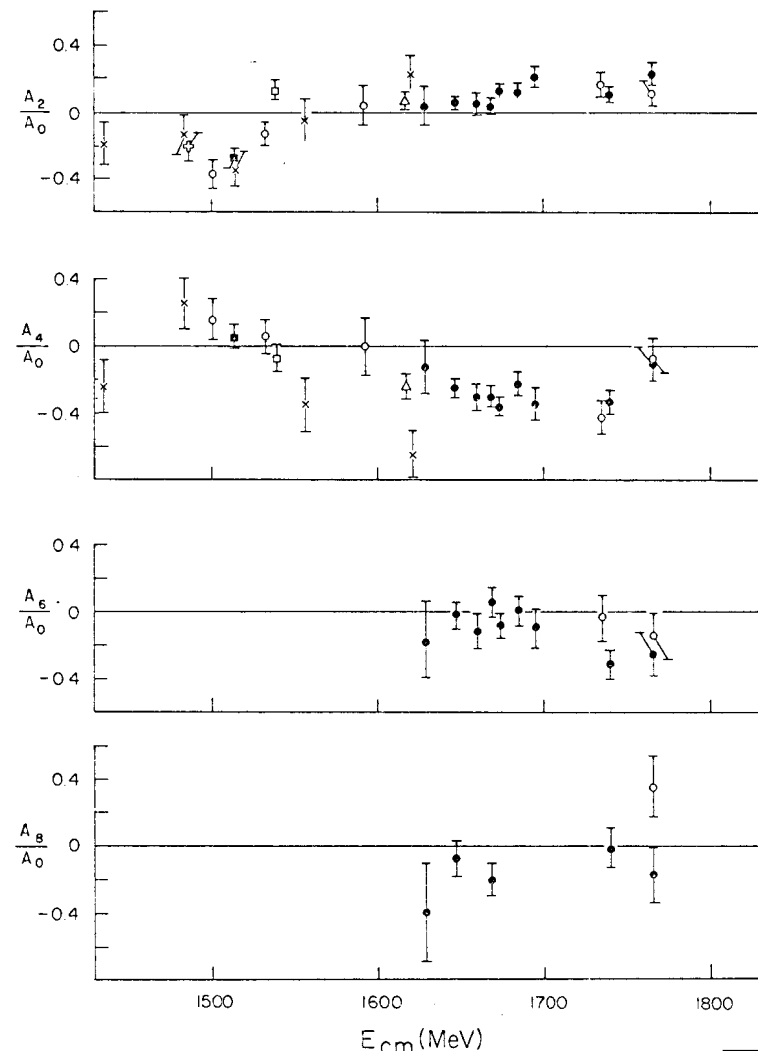
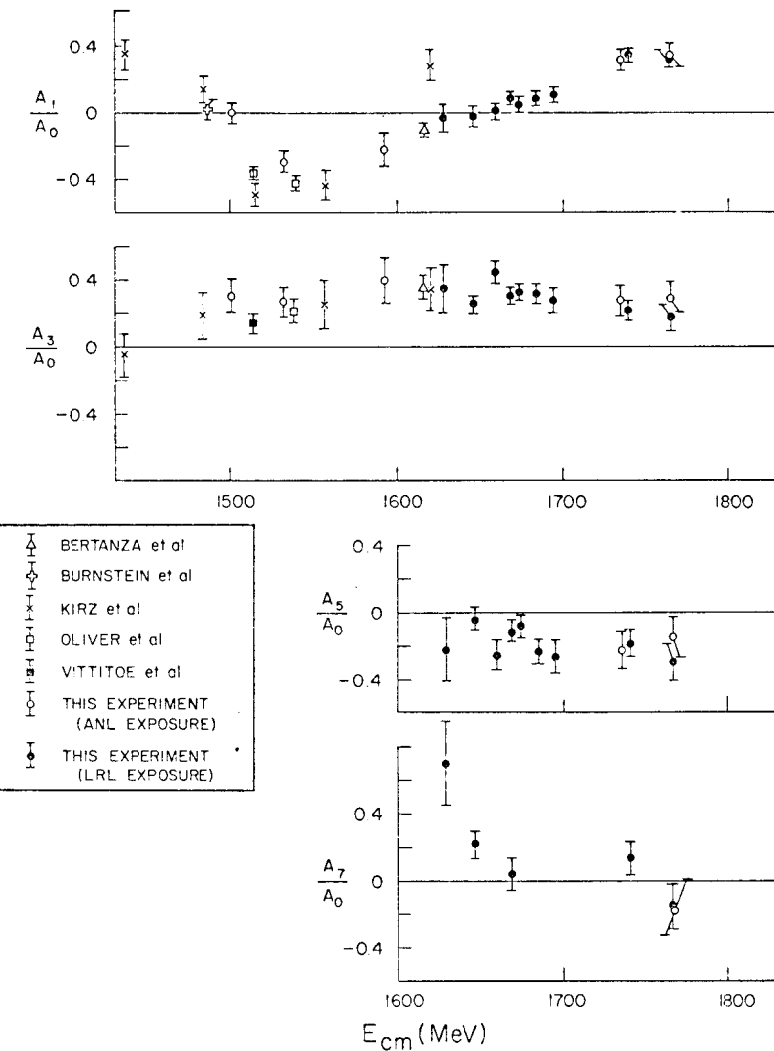


Fig. 12

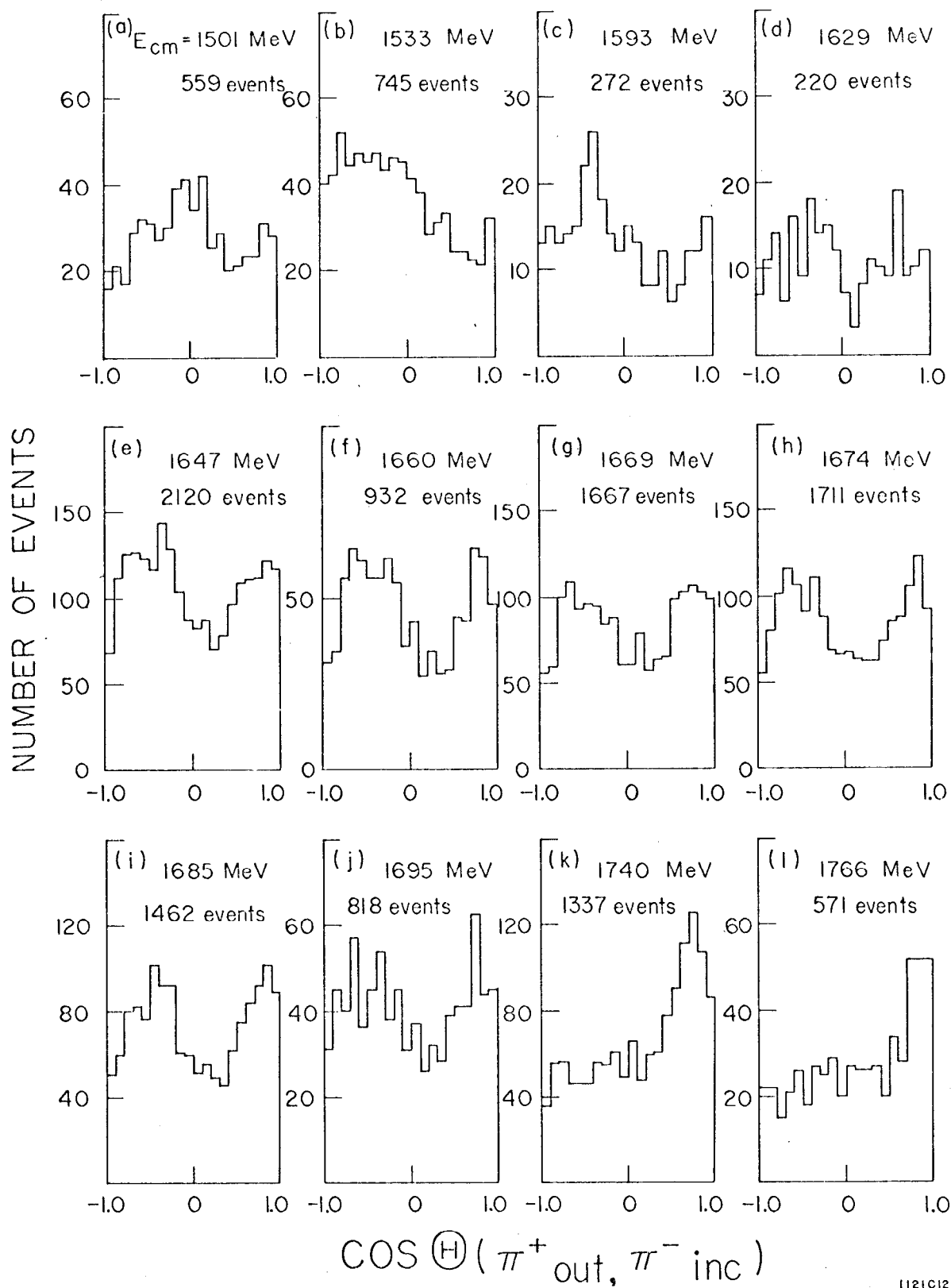
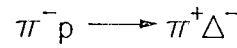
$$\pi^- p \rightarrow \pi^+ \Delta^- (1236)$$


Fig. 13



$$\frac{d\sigma}{d\Omega} = \sum_{\ell} A_{\ell} P_{\ell} \left(\cos \Theta [\pi_{\text{out}}^+, \pi_{\text{inc}}^-] \right)$$

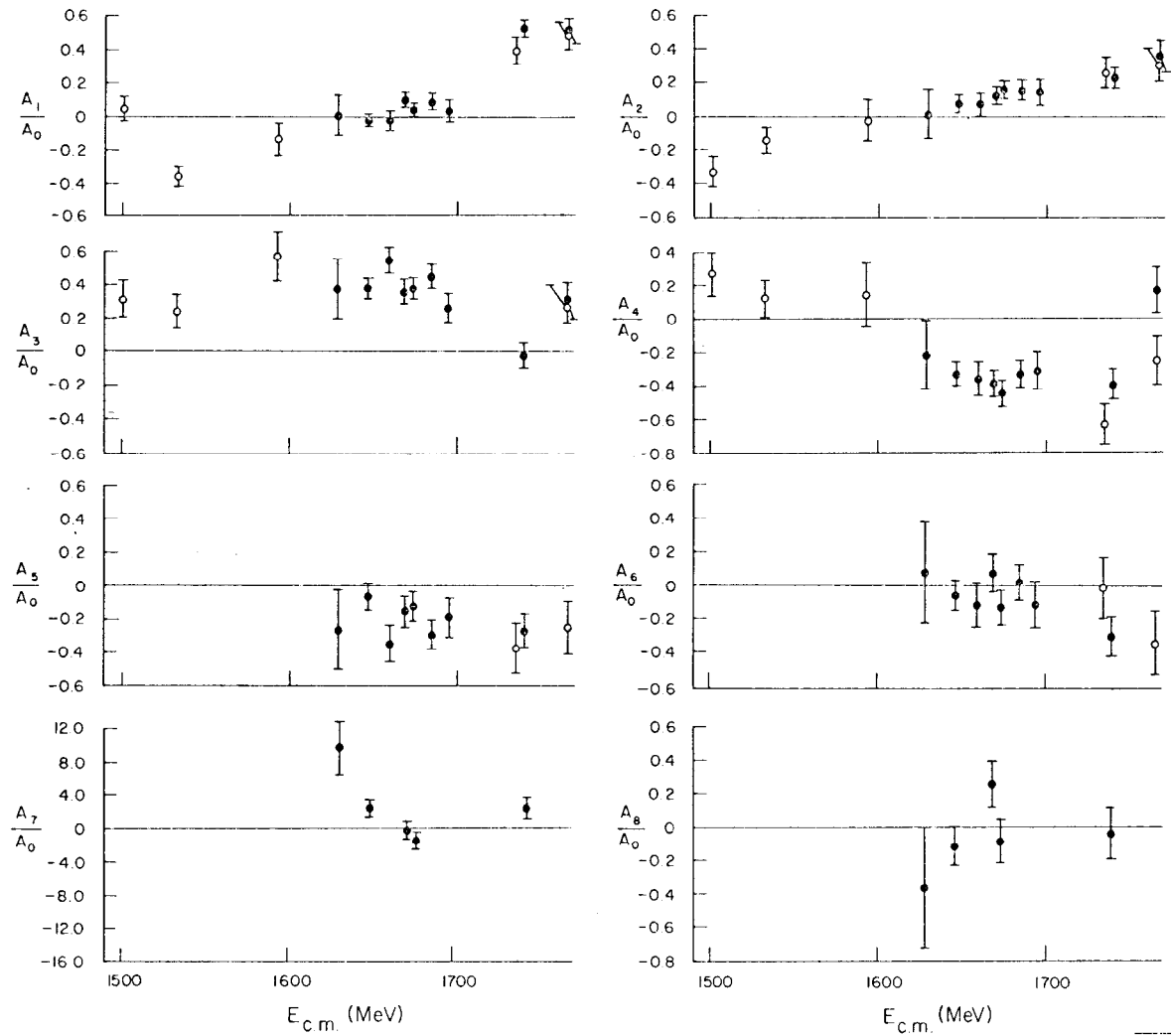


Fig. 14

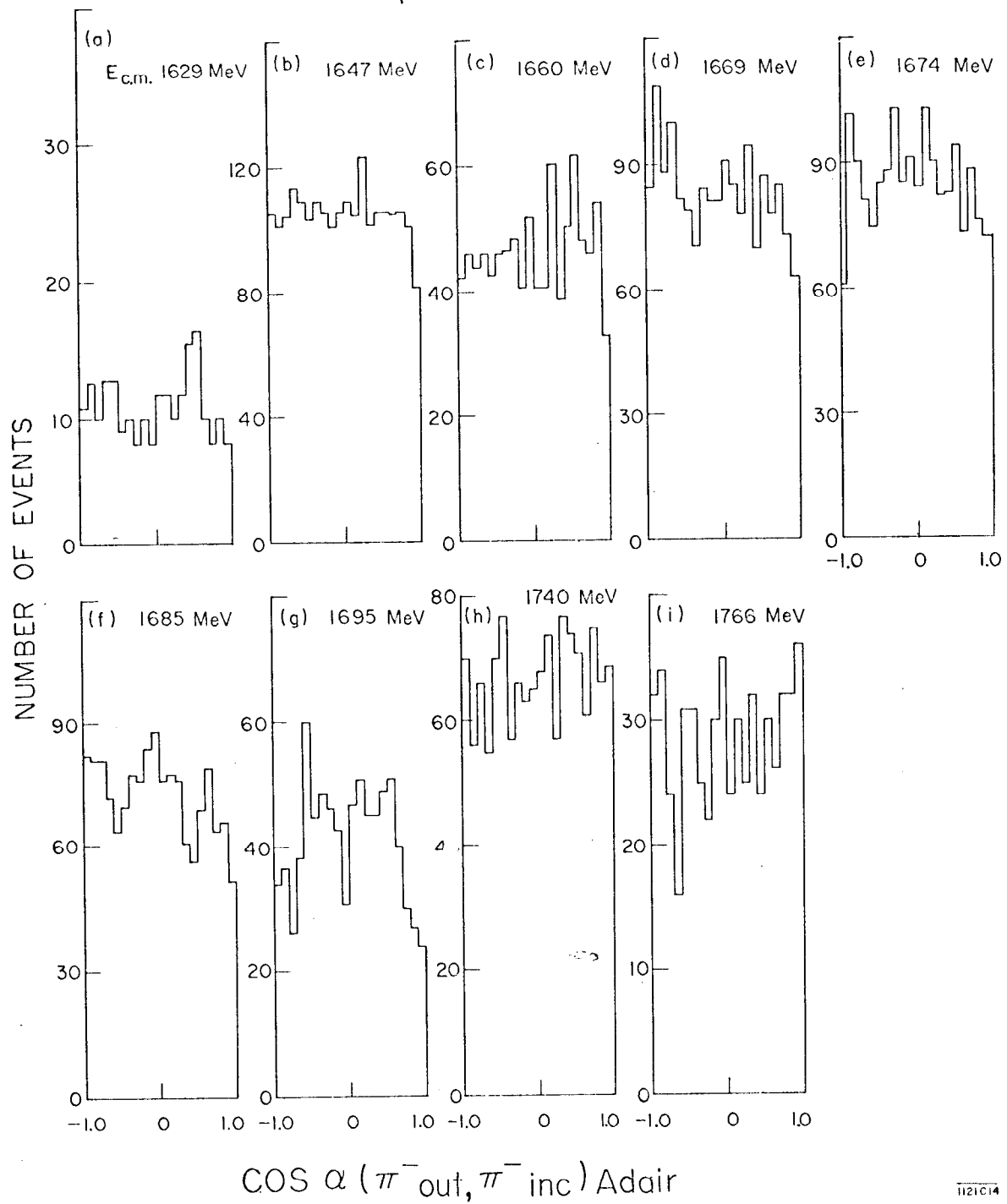
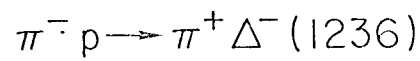


Fig. 15

$\pi^- p \rightarrow \pi^+ \Delta^- (1236) \quad 0.8 \leq \cos \Theta \leq 1.0$

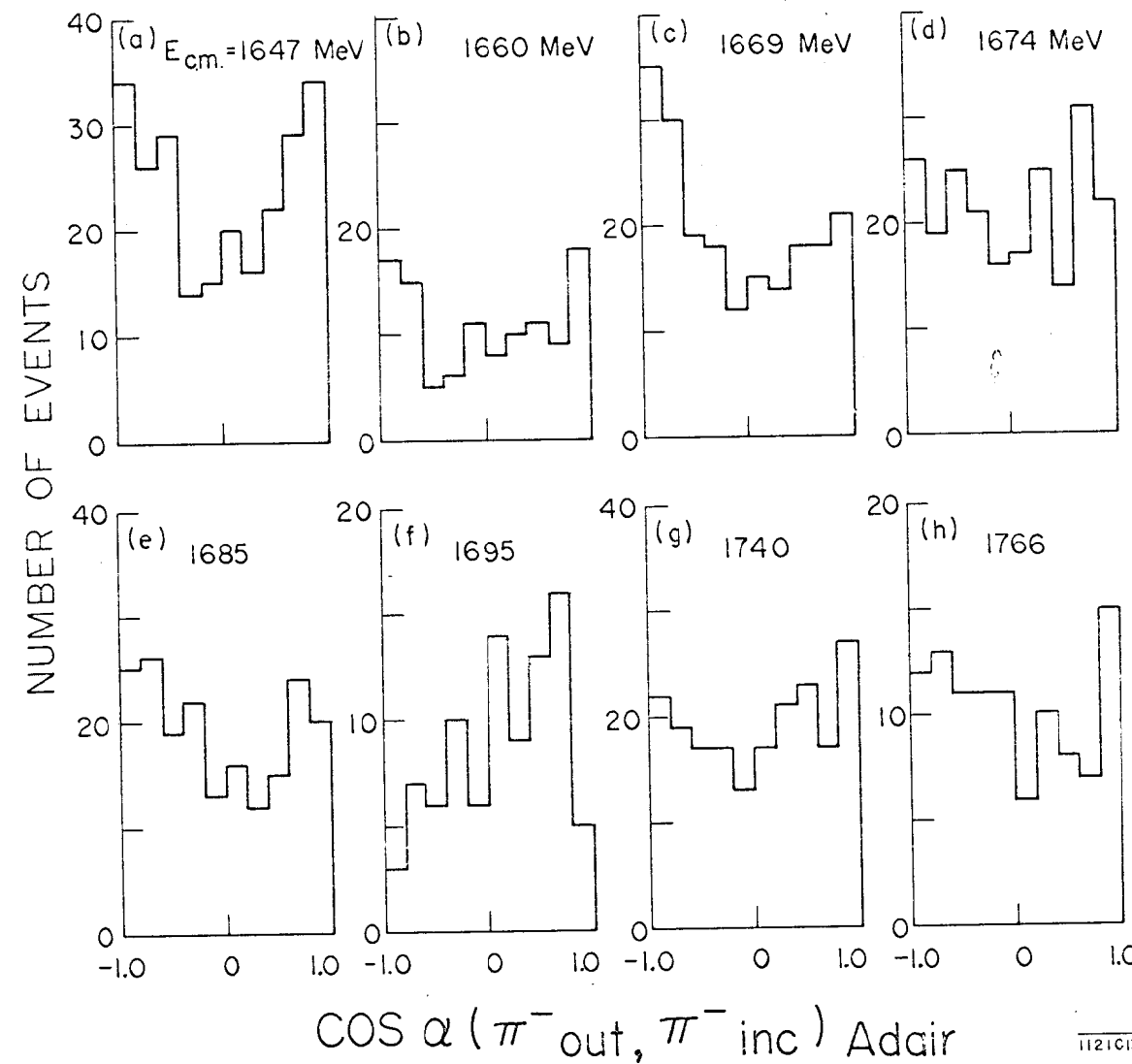


Fig. 16

112103